

A Broad Band and Large Area X-Ray Omni Sky Monitor (BLOSM) ¹

W. Zhang, R. Petre, A. N. Peele¹, K. Jahoda, F. E. Marshall, Y. Soong², and N. E. White

*Laboratory for High Energy Astrophysics
Goddard Space Flight Center
Greenbelt, Greenbelt, MD 20771*

¹ *National Research Council Research Associate*

² *also Universities Space Research Association*

E-mail: William.W.Zhang.1@gssc.nasa.gov

ABSTRACT

We present a conceptual design for a new X-ray all sky monitor (ASM). Compared with previous ASMs, its salient features are: (1) it has a focusing capability that increases the signal to background ratio by a factor of 3; (2) it has a broad-band width: 200 eV to 15 keV; (3) it has a large X-ray collection area: $\sim 10^2 \text{ cm}^2$; (4) it has a duty cycle of nearly 100%, and (5) it can measure the position of a new source with an accuracy of a few minutes of arc. These features combined open up an opportunity for discovering new phenomena as well as monitoring existing phenomena with unprecedented coverage and sensitivity.

Subject headings: Instrumentation: X-ray optics, all sky monitor

¹ Contributed paper to "All-Sky X-Ray Observations in the Next Decade: A Workshop for ASM and GRB Missions in the X-Ray Band, The Institute of Physical and Chemical Research (RIKEN), Wako, Saitama, Japan, March 3-5, 1997.

1. Introduction

ASMs have played an important role in the development of X-ray astronomy. A large number of transients have been discovered and a large number of bright persistent sources have been monitored with them. Their role as watchdog to alert pointing instruments has been most prominent.

Previous all sky monitors suffer from several common shortcomings. First, they are only sensitive to X-rays above 2 keV. Second, they have relatively small effective areas or very small time-averaged effective areas. Third, they do not have any focusing capability. Combining all these factors, their measurement limit is, at best, of the order of several mCrab in several hours or in one day.

In this paper we further develop a concept originally put forth by Schmitt in 1975. With advances in both X-ray optics and detector technology in the past two decades, this concept now is feasible. We will present simulations to show the salient features of such an ASM. It can either fly as a small free-flyer or as one of instruments on a large satellite as previous ASMs.

Table 1 summarizes the most important characteristics of past ASMs. The last row shows the expected capabilities of BLOSM. It represents a significant step in improving the capability and sensitivity of X-ray ASM.

2. Instrument and Mission Concept

The large field of view (FOV) optic proposed by Schmitt in 1975 is focusing in one dimension (see Peele *et al.* 1997 for an illustration of this optic) by flat reflectors mounted along the radial directions of a cylinder. With one module, it focuses a point source in its FOV to a line on the focal surface. In our conceptual design here, we will have two modules situated in perpendicular orientations so that the two coordinates of a source can be obtained simultaneously.

As shown in Figure 1, the instrument consists of two modules. Module 1 is a cylinder 100 cm in diameter at its outer edge and 50 cm in height. Its focal length is 25 cm. Module 2 is 83% (i.e., 300 out of 360 degrees) of a cylinder 70 cm (i.e., $100/\sqrt{2}$) in diameter and 70 cm in height. Its focal length is 17.5 cm. Module 2 sits about 50 cm away on top of module 1. The 50 cm distance is to ensure that the vanes at the

lower side of module 2 are not blocked by module 1.

For the purpose of discussion in this paper, without loss of generality, we will adopt a fake equatorial coordinate system in which the x -axis points to direction $(\alpha, \delta) = (0^\circ, 0^\circ)$, and y -axis $(90^\circ, 0^\circ)$, and z -axis $(0^\circ, 90^\circ)$, and the sun is in position $(0^\circ, -90^\circ)$, as shown in Figure 1. The cylindrical surface of module 1 is defined by: $x^2 + y^2 = 50^2$ and $-25 < z < 25$, and module 2 by: $y^2 + (z - 135)^2 = 35^2$ and $-35 < x < 35$, where all numbers are in cm. The entire satellite spins around the direction to the sun, which, in the specific coordinate system, corresponds to the z -axis.

The cylindrical position-sensitive detectors need only to measure position along the circumferential direction. Every time interval, each model produces a map similar to Figure 2.

3. Source Mapping Deconvolution

For the purpose of illustration, we need to define two angular variables which correspond to the position of a source on the focal surfaces. For module 1, the angle θ_1 measures from the positive x -axis with y -axis at 90° , i.e., θ_1 is the azimuthal angle of module 1. For module 2, the angle θ_2 measures from the y -axis with the z -axis at 90° , i.e., θ_2 is the azimuthal angle of module 2. These two variables are fixed with respect to the modules.

At time $t = 0$ for a source at (α, δ) , it has the following angles in the two modules:

$$\text{module1} : \theta_1 = \alpha, \quad (1)$$

$$\text{module2} : \theta_2 = \arctan(\cos \delta \sin \alpha, \sin \delta), \quad (2)$$

which should be interpreted as $\sin \theta_2 = \cos \delta \sin \alpha$ and $\cos \theta_2 = \sin \delta$. For example, two sources with identical α , but different δ , will have one image in module 1, but two separate images in module 2. A new source and its two coordinates can be easily identified this way. The rotation of the satellite can be taken into account by replacing α in the above equations with $\alpha - \Omega t$, where Ω is the angular velocity of the satellite, and t time.

4. Angular Resolution, Effective Area, and Background

In the ideal case where reflectors are infinitely thin and they are mounted perfectly along their local radial directions, the angular resolution of the system is

the same as the angle between two adjacent reflectors. Figure 3 compares the ideal situation and a realistic situation where the reflector thickness is 0.05 cm. In both cases the angular spacing and other dimensions are the same.

Assuming that the mirrors are coated with Ni with perfect smoothness and the length of each reflector along the radial direction is 3.3 cm (see Peele *et al.* 1997) for module 1, Figure 4 shows the effective area of module 1 as a function of energy for a source perpendicular to the z -axis. Module 2 has exactly the same effective area for a source perpendicular to the z -axis. Though its radius is smaller by a factor of $\sqrt{2}$, it is longer by the same factor.

There are three sources of background: (1) detector internal (non-Xray) background, (2) background contribution from sources in the same annulus of the sky that share the same spot on the focal surface, and (3) the diffuse X-ray background. For the system as outlined in this paper, the detector internal background is much lower than the other two, thus we will ignore it for now. The background contributions of other sources, equivalent to source confusion, though complicated, should not be a problem for relatively bright sources. For the purpose of this paper, we will only consider the diffuse X-ray background.

The diffuse X-ray background flux can be parameterized (Priedhorsky *et al.* 1996) as

$$f = 20E^{-1.89} \quad 0.05 \leq E \leq 0.44 \text{ keV}, \quad (3)$$

$$16E^{-2.16} \quad 0.44 \leq E \leq 2.23 \text{ keV}, \quad (4)$$

$$9.2E^{-1.47} \quad 2.23 \text{ keV} \leq E, \quad (5)$$

where E is in keV and f in $photons/cm^2/s/sr$. The result of simulations with this flux is shown in Figure 5.

5. Practical Considerations

We have been systematically investigating different materials to characterize their suitability as reflectors. We have studied Mylar, Kapton, and PlexiGlas and have found that those materials, even though they can be made very thin and strong, do not satisfy flatness requirements. We have found that thin glass (0.05 cm) which is commercially produced for flat-panel LCD displays has the desired flatness. We have optically tested a few pieces and found that, even though not all of them satisfy the flatness requirements, a significant fraction of them have flatness better than one

minute of arc. We are continuing this investigation to identify the best material. For the purpose of this paper, we will assume that we use glass reflectors with a thickness of 0.05 cm. The angular spacing between two adjacent reflectors is assumed to be 10 minutes of arc, which corresponds to a linear distance of 0.12 and 0.08 cm for modules 1 and 2, respectively. These linear spacings are quite comfortable for mechanically mounting those reflectors to a structure.

In general, these glass sheets are quite smooth. Coated with either gold or nickel, their measured X-ray reflectivity is nearly identical to theoretical expectations.

A challenging part of the building the system as outlined in this paper is the detectors. We require two detectors each with an active area on the order of 7,000 cm^2 . They must have thin window and good one-dimensional position resolution. We have been investigating the possibility of using the micro-strip proportional counter technology. The glass plate will have anode and cathode traces laid on them photolithographically with a pitch of, say, 300 μm . Each trace is read out by its own analog electronics to achieve maximum position resolution. Since we do not require position resolution along the longitudinal directions of the cylinders, the readout electronics can be made simple.

With all these parameters, Table 2 list the key components of this system and their estimated masses.

6. Scientific Merits

Like previous ASMs, BLOSM is capable of monitoring long-term behavior of bright sources. But the most significant aspect of BLOSM is that it covers the soft band below 2 keV and its coverage of every part of the sky except for sources within 30° of the sun. With these two features, we expect it to discover many fast (lasting on the order of seconds or minutes) and/or soft transients. In this section, we give quantitative estimates of BLOSM count rates for several known phenomena. Note that in doing these estimates, we will assume the source is ‘on-axis,’ i.e., it is in a direction perpendicular to the symmetry axis of module 1. The count rates are for module 1 only. For a source that is not on-axis, it may get more or less counts than these estimates, depending on its position. Figure 6 shows how the effective area varies as a function of sun angle, where a factor of 1 corresponds to the estimate here.

1. As a point of reference, we have included the expected count rates from the Crab nebular/pulsar. We have used a power law spectrum with a photon index of -2.05 and an $n_H = 3.0 \times 10^{21} \text{cm}^{-2}$.
2. Gamma Ray Bursts: Since their discovery nearly three decades ago, gamma ray bursts have been the most enigmatic astrophysical phenomenon. It has been generally agreed upon in the last few years that one of potentially very useful measurements is to measure the galactic absorption at low energies. For the estimates in Table 3, we have used the flux measured with the Ginga gamma ray burst detector (T.E. Strohmayer, personal communication) which corresponds to the spectral characterization of Band *et al.* (1993) with $\alpha = -0.9, \beta = -5.0, E_0 = 100 \text{keV}$, and $A = 0.5$. We have considered two cases. In the first case, we extrapolate this spectrum all the way down to 0.1 keV with no interstellar absorption. In the second case, we have assumed an interstellar absorption corresponding to $n_H = 5 \times 10^{22} \text{cm}^{-2}$ and the Morrison and McCammon (1983) cross sections. It is clear that BLOSM is well suited for differentiating the galactic and extra-galactic origin theories of gamma ray bursts.
3. BLOSM is perhaps the first ASM capable of systematic detection of X-ray bursts from galactic sources. Of the 120 or so cataloged galactic low mass X-ray binaries, only 40 or so have been observed to emit Type-I bursts. With a few years of operation, BLOSM should be able to detect X-ray bursts from most of these sources. On the other hand, if no Type-I bursts are detected from a significant number of those sources, it may indicate that some of them may very well be black hole systems. For the estimates in Table 3, we have assumed that the neutron star has a radius of 10 km and is at a distance of 10 kpc. It is clear that BLOSM can detect most of Type-I X-ray bursts. With its position measurement accuracy of 0.1 degrees, BLOSM can associate detected bursts with their persistent counterparts.
4. Active Galactic Nuclei: Long-term variability of AGNs has been the subject of intense organized campaigns in recent years. In Table 3 we show the BLOSM count rate for a 1 mCrab AGN. The spectrum we have used is a power law with

a photon index of -1.7 with $n_H = 3.0 \times 10^{20} \text{cm}^{-2}$ (Mushotzky *et al.* 1993). It takes about 50,000 seconds of observation to detect a 1 mCrab AGN at 10σ level. Therefore BLOSM probably can monitor a few bright AGNs on a daily basis.

5. WGA Catalog/ROSAT Transients: A large number of soft transients have been detected by ROSAT during its observations in the last five years (White 1997 and Angelini, Giommi, & White 1996). With its all sky coverage, BLOSM is expected to detect the brighter ones and monitor them on a daily basis. For example, for a source with a flux of $1.6 \times 10^{-11} \text{ergs/s/cm}^2$ at the detector in the band of 0.5-1.5 keV, BLOSM will detect 0.1 counts/s over a background of 4 counts/s.

7. Conclusion

In summary, we have demonstrated that a one-dimensional focusing all sky monitor as outlined in this paper stands a significant step forward in the direction of larger area and true all sky coverage. Compared with previously-flown and currently flying ASMs, its improvement in source location precision and monitoring sensitivity is well over an order of magnitude. In addition to the capabilities of traditional X-ray all sky monitors, it is capable of detecting gamma ray bursts, soft transients, X-ray bursts, and monitoring a number of AGNs on a daily basis. We conclude by pointing out that the instrument as outlined here is suitable to fly either as a free flyer, such as a small explorer, or as one of many instruments on a larger satellite.

Acknowledgment

We would like to thank Scott Murphy for help in preparing this paper.

References

- L. Angelini, P. Giommi, and N.E. White, 1996, in *Rontgendtrahlung from the Universe*, ed. H.U. Zimmermann, J.E. Trumper, and H. York, pp. 645-646.
- D. Band *et al.* , 1993, ApJ, Vol 413, p. 281.
- R. Morrison and D. McCammon, 1983, ApJ. Vol. 270, pp.119-112.

R.F. Mushotzky, C. Done, and K.A. Pounds, 1993, in *Annu. Rev. Astron. Astrophys.*, Vol. 31, pp. 717-761.

A. Peele *et al.* 1997, in these proceedings.

W.C. Priedhorsky, A.G. Peele, and K.A. Nugent, 1996, *MNRAS*, Vol. 279, pp. 733-750.

W.K.H. Schmidt 1975, *Nucl. Instr. Methods*, Vol. 127, pp. 285-292.

N.E. White 1997, in these proceedings.

J.J.M. in t Zand *et al.* 1994, *SPIE Proceedings*, Vol. 2279, pp. 458-468.

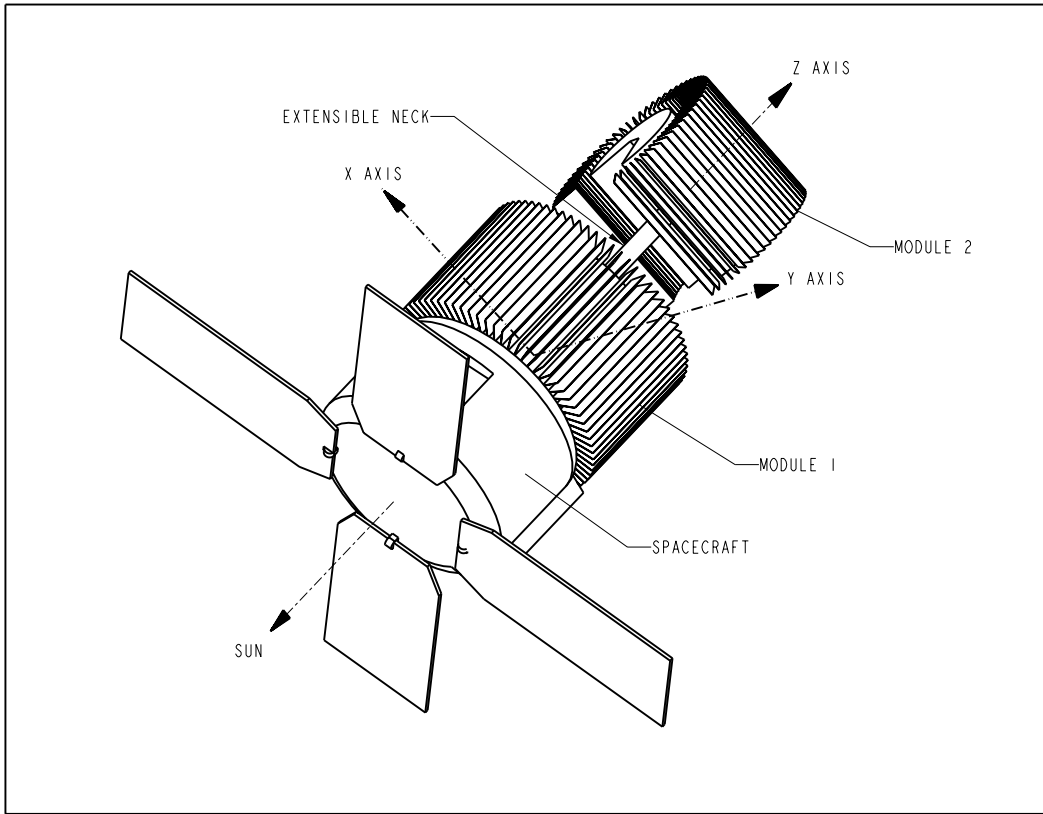


Fig. 1.— Conceptual configuration of a free flyer that carries the all sky monitor described in this paper. With the parameters in this paper, the entire satellite here fits in the latest NASA Small Explorer envelope. The extensible neck is meant to be compressed at launch and extended after launch.

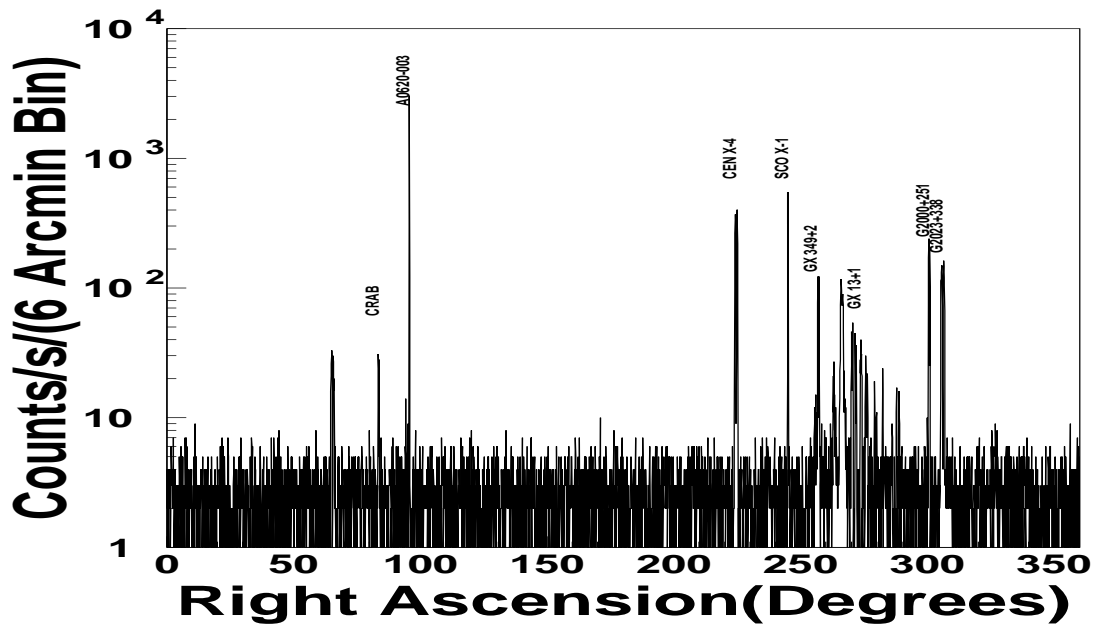


Fig. 2.— A snap shot of the sky with one second of observation. In the fake equatorial coordinate system adopted here, the right ascension coincides with the azimuthal angle along the circumference of module 1.

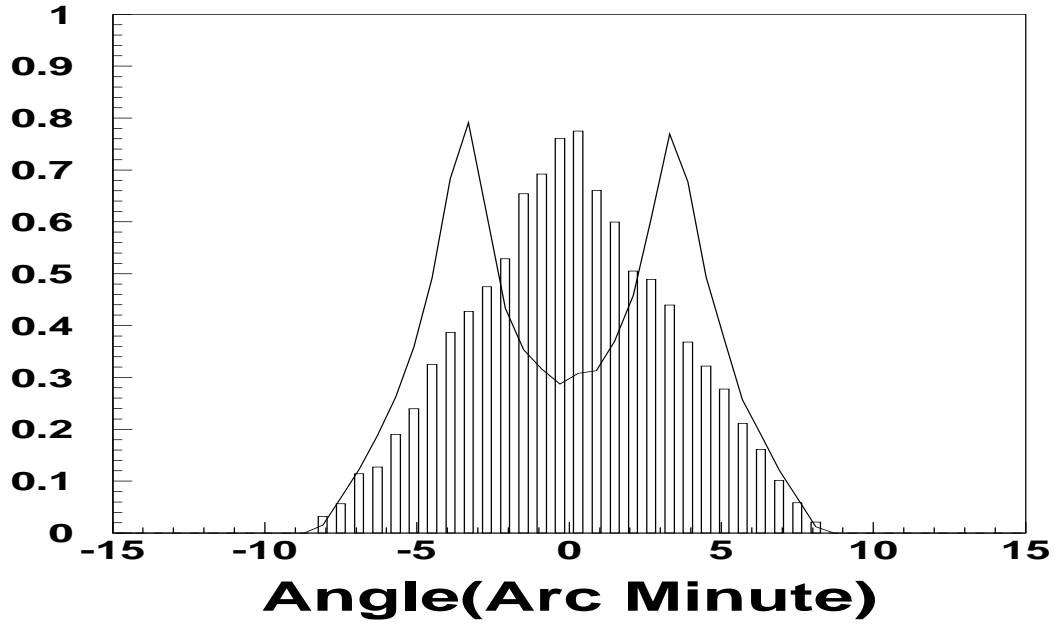


Fig. 3.— Comparison of images achieved with reflectors with no thickness and with thickness of 0.05 cm which is realistically achievable. In both cases, the linear distance between two adjacent reflectors is 0.123 cm and the radius of the cylinder 50 cm.

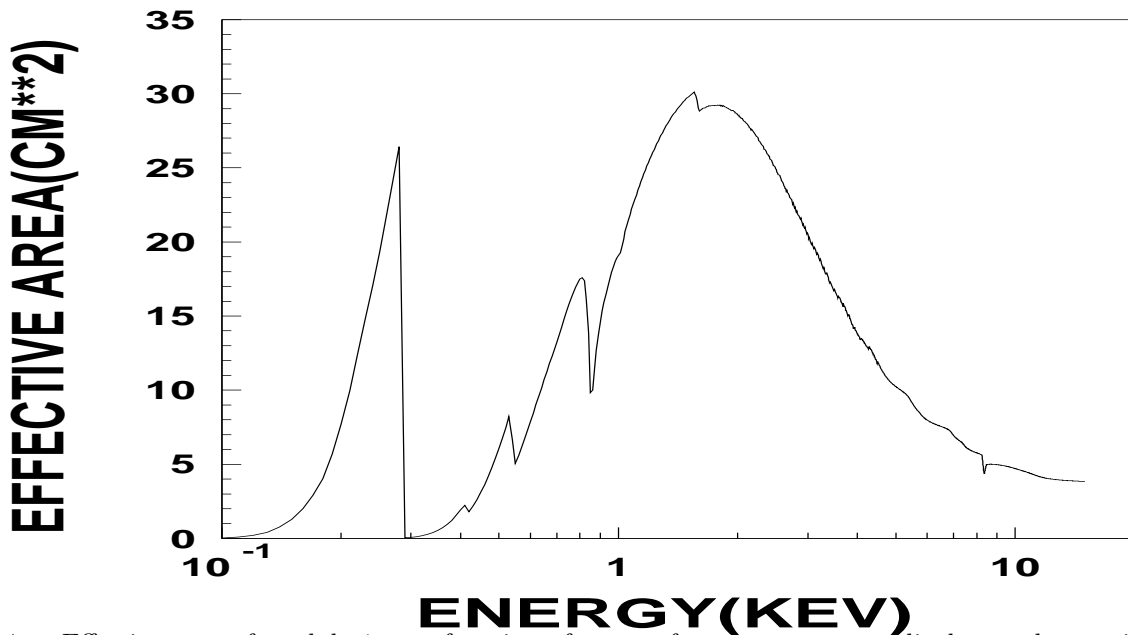


Fig. 4.— Effective area of module 1 as a function of energy for a source perpendicular to the z -axis. We have assumed the window is the same as in Priedhorsky, Peele, and Nugent (1996).

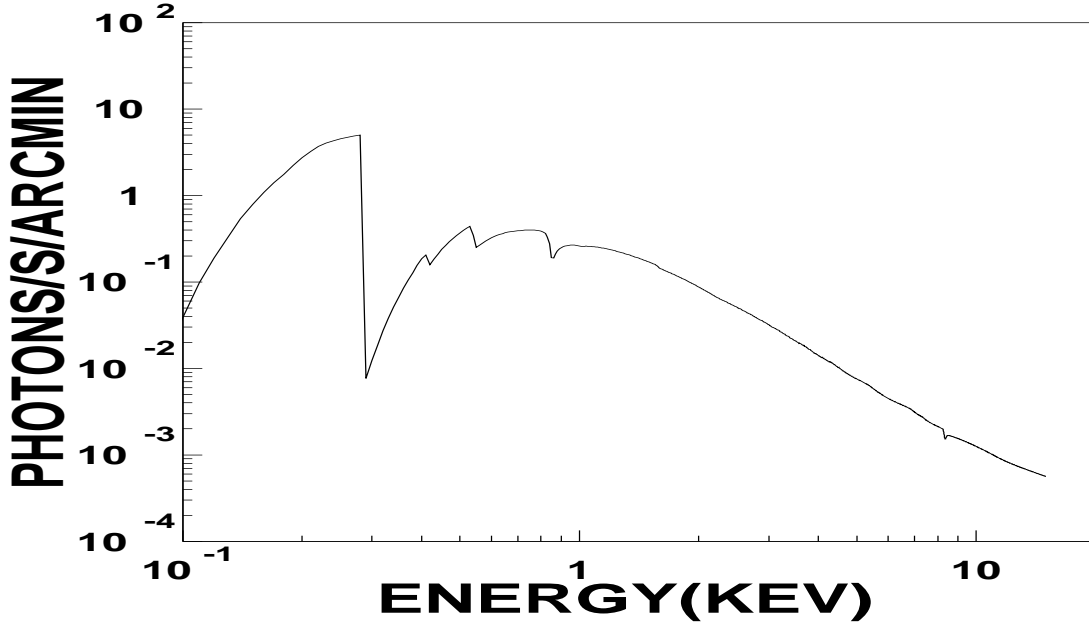


Fig. 5.— Background event rate as a function of energy for module 1. Note here the unit of the ordinate is *photons/s/ArcMin*. For the optimal parameters used in this paper, one should use a 15 ArcMin angular size to estimate background.

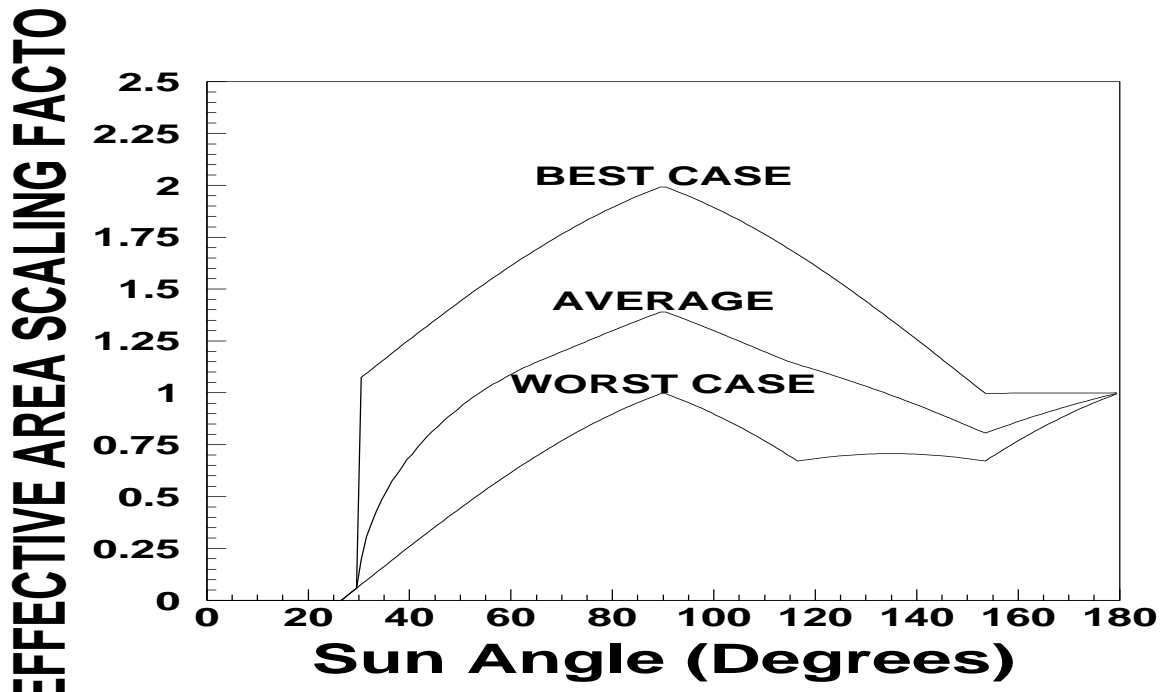


Fig. 6.— Effective area scaling factor as a function of sun angle. The effective area of BLOSM at a given energy for a source is the product of this factor with the corresponding area in Figure 4.

Table 1: Key parameters of past, present, and future X-ray all sky monitors. Adapted with modifications from in t Zand *et al.* For MOXE and BLOSM, both of which have true all sky coverage, their sensitivities correspond to 1.5 hours observations. For others, the sensitivity column corresponds to the time required to cover 75% of the sky.

Instrument	Operational Period	Instantaneous Sky Coverage	Angular Resolution ($^{\circ}$)	Bandpass (keV)	Sensitivity (mCrab)
Vela 5B XC	1969-1979	5×10^{-4}	6.1	3-12	400
Ariel V ASM	1974-1980	1×10^{-2}	10	3-6	170
Ginga ASM	1987-1991	5×10^{-4}	0.2	2-20	50
Watch/Granat	1989-	1	2	6-180	100
BATSE/CGRO	1990-	1	6	20-100	60
ASM/RXTE	1996-	5×10^{-2}	0.2	2-10	20
MOXE/SXG	1997-	1	1.1	2-25	7
BLOSM	?-	1	0.1	0.2-15	1

Table 2: Rough estimates of the masses of BLOSM key components.

Component	Mass (kg)
Optics	130
Detectors	85
Electronics	20
Spacecraft	125
Total	360

Table 3: Effective areas, background count rates, and source count rates in various energy bands.

Source	0.1-0.5 keV (cps)	0.5-2 keV (cps)	2-10 keV (cps)
Background	7.3	5.0	1.5
Crab Nebula	1.2	123	62
GRB ($n_H = 0$)	225	860	772
GRB ($n_H=5E22$)	0	17	423
XRB ($kT = 1keV$)	0	0.06	1.2
XRB ($kT = 2keV$)	0	0.21	11.5
XRB ($kT = 3keV$)	0	0.37	30.8
AGN (1 mCrab)	0	0.1	0.06